JOURNAL OF PROPULSION AND POWER
Vol. 17, No. 5, September–October 2001

Ignition and Flame Studies for an Accelerating Transonic Mixing Layer

X. Fang,* F. Liu,† and W. A. Sirignano‡
University of California, Irvine, California 92697-3975

Numerical solutions have been obtained for a diffusion flame in the two-dimensional, laminar, steady, viscous, multicomponent, compressible mixing layer in the presence of a pressure gradient by using the boundary-layer approximations and solving the *x*-momentum, energy, and species conservation equations. The numerical solutions have been validated against similarity solutions and then are extended to cases where no similarity solution exists. The numerical solutions are used to study the ignition process and the flame structure in an accelerating transonic mixing layer. It is shown how ignition length depends on initial temperature, initial pressure, initial velocity, viscosity, and pressure gradient. Ignition is found to occur on the high-temperature-air side. Oxidation kinetics and transport are both controlling in the upstream ignition region. Farther downstream, transport is controlling in the fully established flame. The boundary-layer approximation is found to be valid everywhere including the upstream ignition region.

Nomenclature

c_p	=	specific heat
D	=	mass diffusivity
H	=	stagnation enthalpy
H_s	=	sensible stagnation enthalpy
h	=	enthalpy
h_t	=	total enthalpy
h^0	=	heat of formation
K	=	ratio of the freestream velocities, $u_\infty/u_{-\infty}$
M	=	Mach number
N	=	total number of species
Pr	=	Prandtl number
p	=	pressure
R	=	gas constant
Sc	=	Schmidt number
T	=	temperature
u	=	velocity in x direction
u_∞	=	dimensional freestream velocity (characteristic velocity)
$u_{-\infty}$	=	dimensional freestream velocity
v	=	velocity in y direction
W	=	molecular weight
x, y	=	Cartesian coordinates
x_{ch}	=	chemical distance, $\rho u/A \exp(-E_a/RT)[\mathrm{fuel}]^a[\mathrm{O_2}]^b$
Y_i	=	mass fraction
Z	=	Schvab–Zel'dovich variable
β_M	=	acceleration parameter
η	=	similarity variable
λ	=	thermal conductivity
μ	=	coefficient of viscosity
ν	=	stoichiometric coefficient
$\bar{\xi}$	=	similarity variable
ρ	=	density
$\dot{\omega}$	=	reaction rate

Subscripts

F	=	fuel
i	=	species (O_2, N_2, H_2O, CO_2, or CH_4)
ig	=	ignition
j	=	species (air or fuel)
ref	=	quantity at reference condition
∞	=	quantity at the top far away from the layer
$-\infty$	=	quantity at the bottom far away from the layer

I. Introduction

THE objective of this study is to analyze some of the issues related to a new technology concerned with the acceleration of reacting flows. One application concerns gas-turbine engines; designers are attempting to increase the thrust-to-weight ratio and to widen the range of engine operation. One major consequence is that the combustor residence time can become shorter than the time required to complete combustion. Therefore, combustion would occur in the turbine passage. A significant benefit can result from augmented burning in the turbine. Liu and Sirignano[1] and Sirignano and Liu[2] have shown by thermodynamic analysis that augmented combustion in the aircraft turbojet engine allows for 1) a reduction in afterburner length and weight, 2) a reduction in specific fuel consumption, and 3) an increase in specific thrust. The increase in specific thrust implies that larger thrust can be achieved with the same cross section or that the same thrust can be achieved with a smaller cross section (and, therefore, still smaller weight). For the ground-based gas turbine, benefits have been shown by thermodynamic analysis to occur in power/weight and efficiencies.[1] A mixing and exothermic chemical reaction in the accelerating flow through the turbine passage offers, therefore, an opportunity for a major technological improvement. The gas-turbine engine is not the only potential application for this technology. The reduction in peak temperatures due to acceleration results in the promise of reduced pollutant formation and reduced heat transfer losses in many other combustion applications.

There is a lack of fundamental treatment in the literature of multidimensional flows with mixing and chemical reaction in the presence of strong pressure gradients that support a transonic flow. For zero pressure gradients, reacting, multidimensional (laminar and turbulent) low Mach number mixing and boundary-layer flows have been considered by many investigators using a wide variety of approaches: see, for example, Marble and Adamson,[3] Emmons,[4] Chung,[5] and Sharma and Sirignano[6] for laminar flows and Patankar and Spalding,[7] Razdan and Kuo,[8] and Givi et al.[9] for

Presented as Paper 2000-0437 at the AIAA 38th Aerospace Sciences Meeting, 8 Exhibit, Reno, NV, 10–13 January 2000; received 1 July 2000; revision received 27 April 2001; accepted for publication 12 June 2001.

*Graduate Student Researcher, Department of Mechanical and Aerospace Engineering.

†Associate Professor, Department of Mechanical and Aerospace Engineering. Senior Member AIAA.

‡Professor, Department of Mechanical and Aerospace Engineering. Fellow AIAA.

turbulent flows. A limited number of efforts have been made on reacting supersonic flows: see, for example, Buckmaster et al.,[10] Grosch and Jackson,[11] Jackson and Hussaini,[12] Im et al.,[13,14] and Chakraborty et al.[15] For a two-dimensional, laminar, nonreacting boundary layer over a solid body with a pressure gradient, similarity solutions were obtained by Li and Nagamatsu,[16] Cohen,[17] and Cohen and Reshotko,[18] who solved the momentum and energy equations transformed by the Illingworth–Stewartson transformation: see Illingworth,[19] Stewartson,[20] and Schlichting.[21]

Sirignano and Kim[22] reduced the partial-differentialequations to a system of ordinary differential equations and obtained similarity solutions for laminar, two-dimensional, mixing, reacting and nonreacting layers with a pressure gradient that accelerates the flow in the direction of the primary stream. These similarity solutions offer some insight into the effect of flow acceleration on the flame structure in the mixing layer. However, they are only valid for restricted classes of flows with certain particular pressure gradients. Moreover, they are not capable to predict the ignition process close to the trailing edge of the splitter plate.

Although the analysis is motivated by applications to the gas-turbine engine, the approach here is to address an idealized problem that has the critical features of mixing and chemical oxidation in a gaseous flow that is accelerating through the transonic range. A mixing layer is considered rather than a channeled elliptic flowfield to simplify the calculations. Similarly, one-step chemical kinetics are taken even though some error occurs when the same scheme is used for both ignition and the established flame. Methane is taken as the fuel because its properties are well documented and it does have application for some ground-based gas-turbine engines. Laminar flow will be considered. In the unexplored problem considered here, these gross simplifications can be allowed while still expecting some useful results and insights. It is believed that some salient characteristics of the flow can be identified with this simplified model. Later, more detailed and more complete analyses can be attempted. In this paper, we develop a finite-difference method for solving the two-dimensional mixing layer equations with chemical reaction without the use of the similarity assumption. We will first compare computational results with the similarity solutions obtained by Sirignano and Kim[22] and then extend our computations to nonsimilar cases to examine the ignition and combustion processes in a general transonic accelerating mixing layer.

II. Governing Equations

Consider a diffusion flame in the two-dimensional, laminar, steady, viscous, multicomponent, compressible mixing layer in the presence of a pressure gradient. At the trailing edge of a flat splitter plate, the hot air mixed with burned gases flowing above the flat plate at the velocity u_∞ comes into contact with a fuel vapor flowing below the flat plate at the velocity $u_{-\infty}$. Then, a chemical reaction takes place between the air and the fuel vapor, and a diffusion flame will be established near the middle of the shear layer.

We are concerned with the ignition and combustion that is established downstream of the point of initial contact between the fuel and airstreams.

After use of the boundary-layer approximations and replacement of the pressure term in the x-momentum equation by the term involving freestream velocity, that is,

$$\rho_\infty u_\infty \frac{\mathrm{d}u_\infty}{\mathrm{d}x} = \rho_{-\infty} u_{-\infty} \frac{\mathrm{d}u_{-\infty}}{\mathrm{d}x} = -\frac{\mathrm{d}p}{\mathrm{d}x} \tag{1}$$

we can write the x-momentum, energy, and species conservation equations as

$$\frac{\partial}{\partial x}\left(\frac{u}{u_\infty}\right) = -\frac{v}{u}\frac{\partial}{\partial y}\left(\frac{u}{u_\infty}\right) + \frac{1}{\rho u}\frac{\partial}{\partial y}\left[\mu\frac{\partial(u/u_\infty)}{\partial y}\right] + \frac{1}{u}\left[\frac{\rho_\infty}{\rho} - \left(\frac{u}{u_\infty}\right)^2\right]\frac{\mathrm{d}u_\infty}{\mathrm{d}x} \tag{2}$$

$$\frac{\partial H}{\partial x} = -\frac{v}{u}\frac{\partial H}{\partial y} + \frac{1}{\rho u Pr}\frac{\partial}{\partial y}\left(\mu\frac{\partial H}{\partial y}\right) + \frac{1}{\rho u}\left(\frac{1}{Sc} - \frac{1}{Pr}\right)\frac{\partial}{\partial y} \tag{3}$$

$$\times\left(\mu\sum_{i=1}^{N} h_{t,i}\frac{\partial Y_i}{\partial y}\right) + \frac{1}{\rho u}\left(1 - \frac{1}{Pr}\right)\frac{\partial}{\partial y}\left[\mu\frac{\partial(u^2/2)}{\partial y}\right] \tag{4}$$

$$\frac{\partial Z_j}{\partial x} = -\frac{v}{u}\frac{\partial Z_j}{\partial y} + \frac{1}{\rho u Sc}\frac{\partial}{\partial y}\left(\mu\frac{\partial Z_j}{\partial y}\right), \qquad j = 1, 2 \tag{5}$$

$$\frac{\partial Y_F}{\partial x} = -\frac{v}{u}\frac{\partial Y_F}{\partial y} + \frac{1}{\rho u Sc}\frac{\partial}{\partial y}\left(\mu\frac{\partial Y_F}{\partial y}\right) + \frac{\dot{\omega}_F}{\rho u} \tag{6}$$

where i denotes O_2, N_2, H_2O, CO_2, and CH_4. The reaction rate $\dot{\omega}_j$ in the species equation has been eliminated by introducing the Schvab–Zel'dovich variables:

$$Z_j = Y_j - \nu_j Y_F, \qquad j = 1, 2 \tag{7}$$

where $j = 1$ denotes air and $j = 2$ denotes products.

The Prandtl number is defined as

$$Pr = c_p\mu/\lambda \tag{8}$$

where λ is thermal conductivity. The Schmidt number is defined as

$$Sc = \mu/\rho D \tag{9}$$

where D is mass diffusivity.

The stagnation enthalpy is defined as

$$H = h_t + \tfrac{1}{2}u^2 \tag{10}$$

and the total enthalpy is

$$h_t = \int_{T_{\mathrm{ref}}}^{T} c_p\,\mathrm{d}T' + \sum_{i=1}^{N} Y_i h_i^0 \tag{11}$$

where h_i^0 is the heat of formation of species i at the reference temperature T_{ref}.

The boundary conditions are specified as $y \to \infty$ as

$$u \longrightarrow u_\infty, \qquad H \longrightarrow H_\infty, \qquad Z_j \longrightarrow Z_{j\infty}$$

and as $y \longrightarrow -\infty$ as

$$u \longrightarrow u_{-\infty}, \qquad H \longrightarrow H_{-\infty}, \qquad Z_j \longrightarrow Z_{j-\infty}$$

A perfect gas is assumed

$$p = \sum_{i=1}^{N} \rho Y_i R_i T \tag{12}$$

In the solution procedure, the average gas constant R, molecular weight W, and viscosity coefficient μ can be obtained by the following equations:

$$R = \sum_{i=1}^{N} R_i Y_i \tag{13}$$

$$\frac{1}{W} = \sum_{i=1}^{N} \frac{1}{W_i} Y_i \tag{14}$$

$$\mu = \sum_{i=1}^{N} \mu_i(T) Y_i \tag{15}$$

The viscosity coefficient of each species μ_i is obtained by using the Sutherland law (see Ref. 23),

$$\mu_i/\mu_0 = (T/T_0)^{\frac{3}{2}}[(T_0 + S)/(T + S)] \tag{16}$$

III. Solution Methods and Constraints

We consider steady, two-dimensional, compressible flow. *Pr* and *Sc* are constant in each case, but they can vary from case to case. In this calculation, we solve five equations, one for the dimensionless velocity u/u_∞, two for the Schvab–Zel'dovich variables Z_{air} and Z_{product}, one for the fuel mass fraction Y_F, and one for the stagnation enthalpy H.

We have developed a two-dimensional, implicit, finite difference algorithm to solve simultaneously the set of the discretized partial-differential equations (PDEs). The method is based on the Crank–Nicolson scheme (see Ref. 24). It is second-order accurate in both the x direction and the y direction.

We first solve for velocity in the x direction, u, temperature T, and mass fractions of all of the species from Eqs. (2), (3), and (5), respectively, by using parameters in the preceding step. Then we calculate density ρ and velocity in the y direction, v, from the equation of state and continuity equation, respectively, using the new solutions. After the solutions at this step have been obtained, we use the mean value of parameters at this step and the preceding step in the next iteration and solve the set of partial differential equations again. We compare the new solutions and the last solutions to see if they are accurate enough. Our accuracy criteria are that the difference between the last two solutions in fuel mass fraction at any grid point in y direction must be less than 1.0×10^{-6} and in temperature must be less than 1.0×10^{-3} K. If both conditions are satisfied, we go to the next x step; otherwise, we iterate again. Normally each step needs 6–10 iterations to satisfy the accuracy criteria.

The momentum balance in the y direction can be expressed as

$$\rho_\infty u_\infty v_\infty = -\rho_{-\infty} u_{-\infty} v_{-\infty} \tag{17}$$

After u has been solved from Eq. (2), v can be obtained by integrating the continuity equation,

$$\rho v = \rho_{-\infty} v_{-\infty} - \int_{-\infty}^{y} \frac{\partial(\rho u)}{\partial x}\, \mathrm{d}y' \tag{18}$$

After H has been solved from Eq. (3), we can calculate temperature by using the following equations:

$$h = \sum_{i=1}^{N} h_i Y_i = \int_{T_{\text{ref}}}^{T} \sum_{i=1}^{N} c_{p_i} Y_i \, \mathrm{d}T' \tag{19}$$

$$h = H - \frac{1}{2}u^2 - \sum_{i=1}^{N} Y_i h_i^0 \tag{20}$$

$$\mathrm{d}h = \sum_{i=1}^{N} h_i \, \mathrm{d}Y_i + \sum_{i=1}^{N} c_{p_i} Y_i \, \mathrm{d}T \tag{21}$$

where

$$c_p = \sum_{i=1}^{N} c_{p_i}(T) Y_i \tag{22}$$

Equation (18) can be rewritten as

$$\mathrm{d}h = \sum_{i=1}^{N} h_i \, \mathrm{d}Y_i + c_p \, \mathrm{d}T \tag{23}$$

from which $\mathrm{d}T$ can be solved, and thus, temperature can be calculated at each point in space.

Methane (CH_4) is used for the current computations, although the method is not restricted to only one type of fuel. The combustion process is described by a one-step overall chemical reaction as

$$CH_4 + 2O_2 + 7.52N_2 \longrightarrow CO_2 + 2H_2O + 7.52N_2$$

The chemical kinetics rate can be described as

$$\dot{\omega}_F = A \exp -(E_a/RT)[\text{fuel}]^a[O_2]^b \tag{24}$$

where [ ] represents molar concentration in mol per cubic centimeter. According to Westbrook et al.,[25] for methane (CH_4), $A = 2.8 \times 10^9$ 1/s, $E_a = 48.4$ kcal/mol, $a = -0.3$, and $b = 1.3$. Note that the kinetic time for mass conversion will be independent of pressure for these values. Although there are quantitative errors in applying this kinetic law to a wide range of temperatures and, in particular, to the ignition event, the qualitative results will be valuable. The trends as key parameters vary will be identified.

IV. Comparison with Similarity Solutions

Sirignano and Kim[22] obtained similarity solutions for a laminar, two-dimensional, mixing, reacting and nonreacting layers with certain prescribed pressure gradients. In this section, we calculate the same similarity cases using the new finite difference method without the similarity assumptions. After obtaining the flowfield, the solution are recast in the same similarity variables and compared with the results by Sirignano and Kim.[22]

Nonreacting Single-Component Case

In this case the fluids below and above the splitter plate are both air but have different velocities and temperatures. Hot air flowing above the flat plate at the velocity u_∞ comes into contact with cold air flowing below the flat plate at the velocity $u_{-\infty}$. Similarity solutions exist for situations where K and β_M are constants.[22] Here, K is the ratio of the freestream velocities $u_\infty/u_{-\infty}$, and β_M is the acceleration parameter,

$$\beta_M = \beta\left\{1 + [(\gamma - 1)/2]M_\infty^2\right\} \tag{25}$$

M_∞ is the Mach number at the top freestream and

$$\beta(\bar{\xi}) = \frac{2\xi}{u_\infty}\frac{\mathrm{d}u_\infty}{\mathrm{d}\bar{\xi}} \tag{26}$$

where $\bar{\xi}$ is a similarity variable

$$\mathrm{d}\bar{\xi} = u_\infty \, \mathrm{d}\xi \tag{27}$$

$$\mathrm{d}\xi = \frac{\rho u}{\rho_0 u_0}\, \mathrm{d}x \tag{28}$$

The subscript 0 refers to stagnation conditions in the freestream, whereas $\beta_M > 0$ means accelerating and $\beta_M < 0$ means decelerating. We compare the solution of the system of PDEs with similarity solutions by Sirignano and Kim[22] for the dimensionless velocity u/u_∞ and the dimensionless sensible stagnation enthalpy $(H_s - H_{s-\infty})/H_{s\infty}$ under the conditions that $K = 5$ and $\beta_M = 1$. Figures 1 and 2 show the dimensionless velocity u/u_∞ and the dimensionless sensible stagnation enthalpy $(H_s - H_{s-\infty})/H_{s\infty}$ vs η, respectively. The close agreement between the numerical solutions and the similarity solutions verifies the accuracy of our computational code.

Reacting Multicomponent Case

In this case, a hot air mixed with burned gases flowing above the flat plate at the velocity u_∞ comes into contact with a fuel vapor mixed with burned gases flowing below the flat plate at the velocity $u_{-\infty}$. Similarity solutions exist again for situations where K and β_M are constants[22] and the reaction rate is infinite.

In this section, we compare the dimensionless velocity u/u_∞ and the dimensionless sensible stagnation enthalpy $(H_s - H_{s-\infty})/H_{s\infty}$

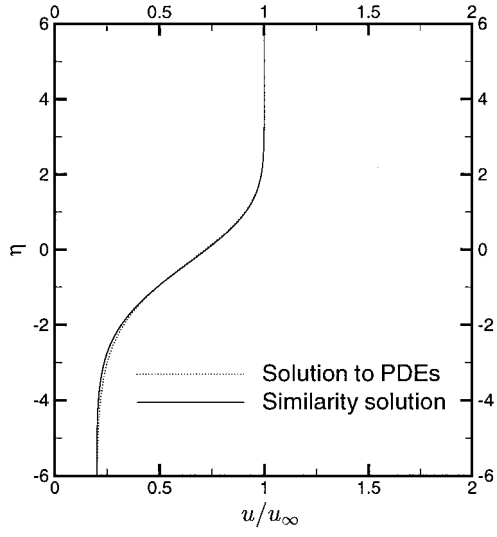

Fig. 1 Dimensionless velocity u/u_∞ vs η for nonreacting similar case $K = 5$ and $\beta_M = 1$; PDE solutions are at $x = 1.53$, 2.89, and 4.76 mm corresponding to $\bar{\xi} = 1$, 2, and 3, respectively.

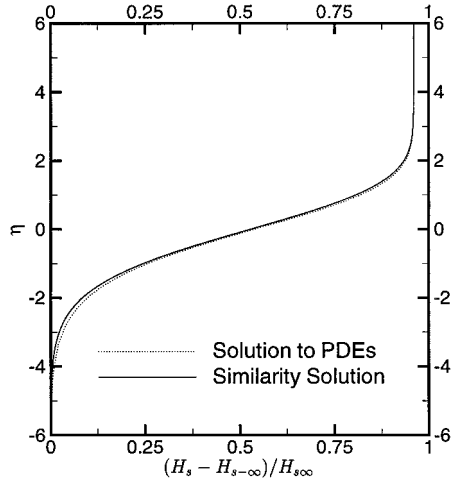

Fig. 2 $(H_s - H_{s-\infty})/H_{s\infty}$ vs η for nonreacting similar case $K = 5$ and $\beta_M = 1$; PDE solutions are at $x = 1.53$, 2.89, and 4.76 mm corresponding to $\bar{\xi} = 1$, 2, and 3, respectively.

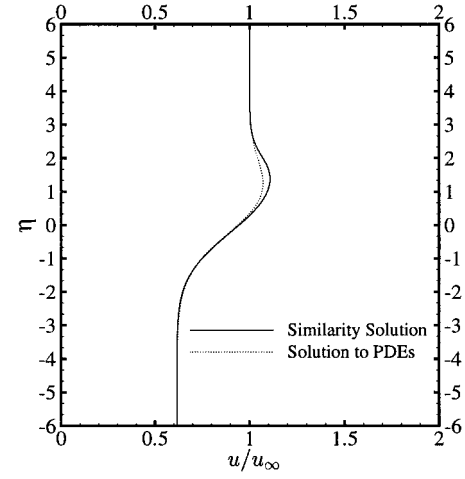

Fig. 3 Dimensionless velocity u/u_∞ vs η for reacting similar case $K = 1.623$ and $\beta_M = 2$; PDE solutions are at $x = 3.16$, 4.89, and 6.02 mm corresponding to $\bar{\xi} = 2$, 3, and 4, respectively.

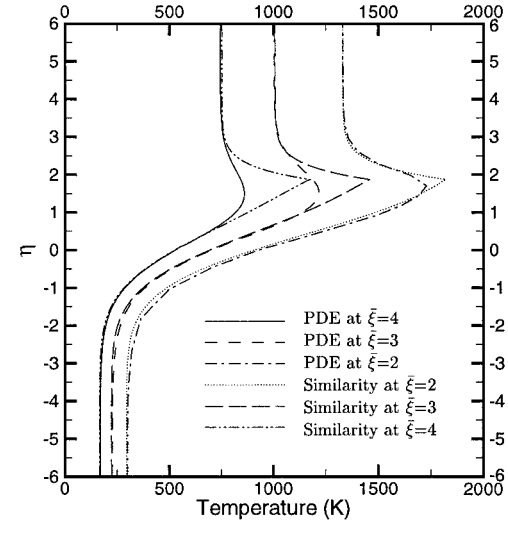

Fig. 4 Temperature vs η for reacting similar case $K = 1.623$ and $\beta_M = 2$; PDE solutions are at $x = 3.16$, 4.89, and 6.02 mm corresponding to $\bar{\xi} = 2$, 3, and 4, respectively.

under the conditions that $K = 1.623$ and $\beta_M = 2$. Figures 3 and 4 show the dimensionless velocity u/u_∞ and temperature vs η, respectively. In the presence of accelerating pressure gradients, the maximum velocity occurs near the middle of the shear layer, where the temperature is high due to the chemical reaction, and thus, the density is low. The low-density regime experiences the greatest acceleration. It is noted that the maximum velocity is lower in the solution of the PDEs than in the similarity solution. In the similarity solution, the model of infinite chemical kinetics rate is used, whereas in the solution of PDEs, we use the actual chemical kinetics rate, which produces a lower peak temperature and a higher minimum density.

Figure 4 shows the temperature vs η at different $\bar{\xi}$ locations. At the same $\bar{\xi}$ position, the maximum temperature is lower in the solution of the PDEs than in the similarity solution due to the use of finite-rate chemistry. As $\bar{\xi}$ increases, the difference becomes more and more obvious because the actual chemical kinetics rate becomes lower and lower.

Calculation with three sets of grids are performed. One base grid has the grid sizes in x and y directions to be $\Delta x = 3.125 \times 10^{-5}$ m and $\Delta y = 1.5 \times 10^{-6}$ m, respectively. Two other grids are formed by using $2\Delta x$ and $2\Delta y$ and $0.5\Delta x$ and $0.5\Delta y$ of the base grid to obtain one coarser grid and one finer grid, respectively. Velocity and temperature profiles obtained by these grids are indistinguishable in graphical presentations, indicating complete grid convergence. To be conservative, however, the results presented in this paper are obtained on grids with $\Delta x = 6.8 \times 10^{-6}$ m and $\Delta y = 0.8 \times 10^{-6}$ m.

V. Nonsimilar Solutions

After validating our numerical method against the similarity solutions, we extend our calculation to cases where no similarity solution exists.

We consider the same reacting case as in Sec. III, where a hot air at the velocity u_∞ comes into contact with a fuel vapor at the velocity $u_{-\infty}$. However, we will remove the similarity conditions that K and β_M are constants. We consider flows with arbitrary freestream velocities and pressure gradients and use finite-rate chemical kinetics where no similarity solution exists.

In this section we study the influence of various flow parameters on ignition and flame structure. Table 1 lists the different cases of study. Cases 1–11 represent a set of studies within which each flow parameter, including the initial air temperature, pressure, and initial air fraction, varies independently relative to the base case (case 1). In a practical application, however, the initial air fraction of the air/fuel mixture coming into the turbine has a dependence on the turbine inlet temperature and pressure because fuel is burned in the main combustor to reach the prescribed temperature. Consequently, the initial temperature or pressure in our studies cannot

Table 1 Parameter survey and ignition length results

Case	T_{air}, K	T_F, K	p_0, atm	dp/dx, atm/m	Y_{air}	u_{air}, m/s	u_F, m/s	Pr	Sc	$\dot{\omega}/\dot{\omega}_{base}$	μ/μ_{base}	x_{ig}, mm
1	1650	400	30	−200	1.0	50	25	1.0	1.0	1.0	1.0	0.448
2	1650	400	30	0	1.0	50	25	1.0	1.0	1.0	1.0	0.416
3	1650	400	30	−350	1.0	50	25	1.0	1.0	1.0	1.0	0.496
4	1650	400	60	−200	1.0	50	25	1.0	1.0	1.0	1.0	0.656
5	1650	400	200	−200	1.0	50	25	1.0	1.0	1.0	1.0	0.384
6	2000	400	30	−200	1.0	50	25	1.0	1.0	1.0	1.0	0.064
7	1650	700	30	−200	1.0	50	25	1.0	1.0	1.0	1.0	3.200
8	1650	400	30	−200	1.0	100	25	1.0	1.0	1.0	1.0	3.440
9	1650	400	30	−200	1.0	50	100	1.0	1.0	1.0	1.0	0.080
10	1650	400	30	−200	1.0	50	25	1.0	1.0	1.0	0.2	0.080
11	1650	400	30	−200	1.0	50	25	1.0	1.0	0.1	1.0	0.432
12	1650	400	30	−200	0.5848	50	25	1.0	1.0	1.0	1.0	0.464
13	1650	400	60	−200	0.6625	50	25	1.0	1.0	1.0	1.0	0.672
14	1650	400	200	−200	0.8500	50	25	1.0	1.0	1.0	1.0	0.512
15	2000	400	30	−200	0.3866	50	25	1.0	1.0	1.0	1.0	0.192

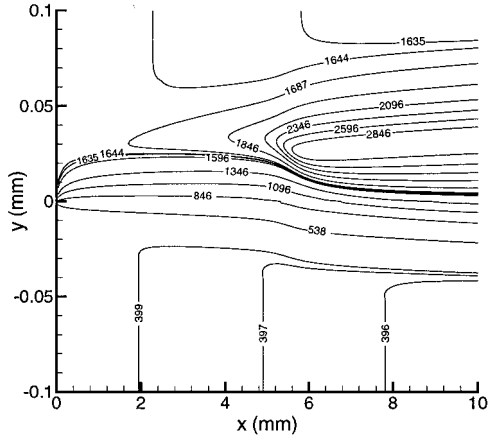

Fig. 5 Temperature contours for case 1 (base case).

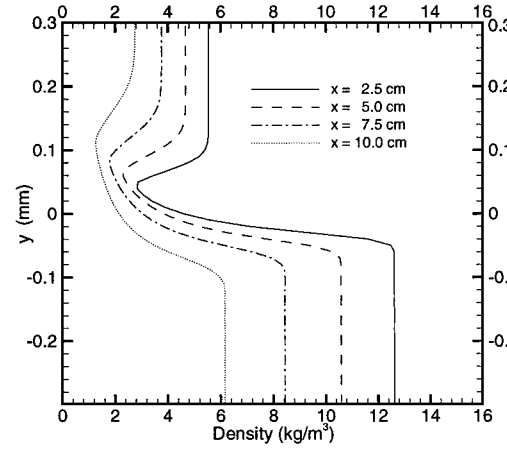

Fig. 6 Density vs y for case 1 (base case).

be realistically varied independently without changing the initial air mass fraction. Therefore, additional cases, cases 12–15, are studied in which variation of initial temperature or pressure is accompanied by a corresponding variation in initial air mass fraction based on a combustion model for the main combustor of a jet engine. These cases will be referred to as the coupled cases and will be presented in Sec. V. Results for cases 1–11, the uncoupled studies, are presented in this section.

Base Case

Figure 5 shows temperature contours under the base case (case 1) parameters. The ignition occurs after a certain distance in the x direction. The peak value of the temperature and the two temperatures at the freestream locations decrease as one moves downstream. The flow accelerates due to the pressure gradient, but the stagnation temperature remains the same; therefore the temperature will decrease in the downstream direction.

The peak value of the temperature occurs at a positive value of y (the air side) and is moving upward when the flow moves downstream. The reason is that the mass of air required in stoichiometric combustion is much greater than that of the fuel. Figure 6 shows the density ρ vs y at four different x positions for the base case. The density curve has a minimum point where the temperature is high, whereas pressure is the same at the same x position. Figure 7 presents the dimensionless velocity u/u_∞ vs y at four different x positions for the base case. The boundary layer becomes thicker, and the ratio $u_{-\infty}/u_\infty$ becomes larger as the flow moves downstream. At the air side, both the density and the velocity are greater than at the fuel (CH_4) side. From the freestream momentum equation (1), the acceleration at the fuel (CH_4) side should be greater than the acceleration at the air side.

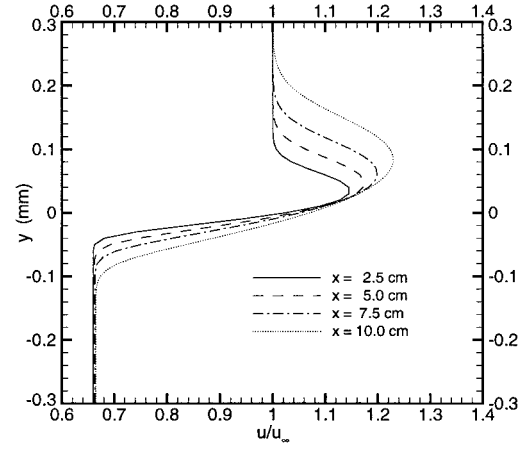

Fig. 7 Dimensionless velocity u/u_∞ vs y for case 1 (base case).

From Fig. 6, the density near the middle of the shear layer is smaller than the density at the two freestreams, and so under the same pressure gradient the acceleration is higher near the middle of the shear layer. Therefore, the dimensionless velocity curve has a peak at the same y position as the density minimum point and the temperature peak. Figure 8 shows the mass fraction vs y at $x = 10.0$ cm for the base case. The peak value of the product mass fraction also occurs at a positive value of y. There is a peak for mass fraction of O_2 in Fig. 8. It occurs because at some y positions the O_2 density due to diffusion is greater than the O_2 consumed by the chemical reaction because at these positions the chemical reaction rate is low. The Mach number has a minimum point where

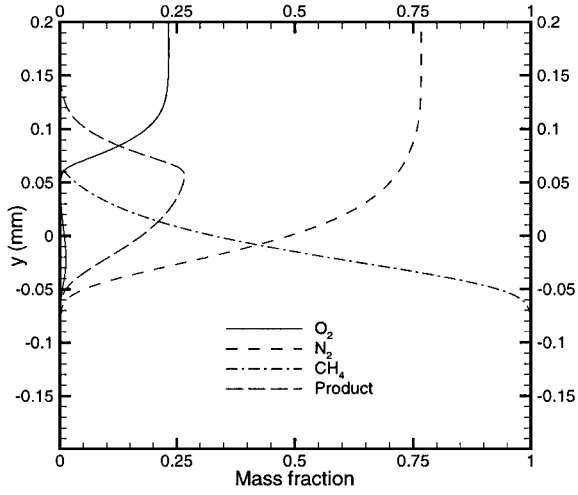

Fig. 8 Mass fraction vs y at $x = 10$ cm for case 1 (base case).

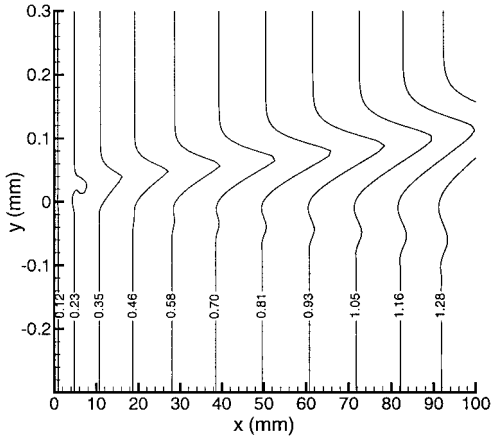

Fig. 9 Mach number contours for case 1 (base case).

the temperature peaks because there the speed of sound is high. This behavior is evident in Fig. 9. There is a local minimum point for Mach number a little below the main minimum point. Near that point, because the temperature is already high, as we move from the fuel side to the air side, the speed of sound is also high, but the velocity increases more slowly than temperature, and the Mach number decreases. At a certain point, the velocity begins to increase very fast, even faster than temperature, so the Mach number begins to increase. In the middle of the flame, the temperature is very high, the Mach number decreases again and forms a minimum point. It is also noticed that in parts of the flow region, for example $x = 7.5$ cm, the flame region is subsonic while the freestreams are supersonic.

Figure 10 shows air consumption rate (kilogram per second square meter) (integral of reaction rate of air over y in a fixed x position) and the corresponding height of air that is consumed by reaction vs x for case 1. The air consumption rate has a maximum point where the reaction rate is the highest over the whole x range. The corresponding height of air shows the height of air that we must supply to make it react efficiently. It has a point where the slope is maximum that is at the same x position as the maximum point in air consumption rate.

Figures 11 and 12 show the reaction rate and product mass fraction vs y at four different x positions for case 1. At the first two x positions, the thickness of the reaction rate and the thickness of product mass fraction are comparable. At the last two x positions, the thickness of the reaction rate does not change much, but the thickness of product mass fraction changes a lot due to diffusion. It is obvious that, in the beginning, reaction rate and diffusion are both controlling, and farther downstream, the diffusion is controlling.

We also calculated the ratio of the diffusion rate in the flow direction to the diffusion rate in the transverse direction. The absolute

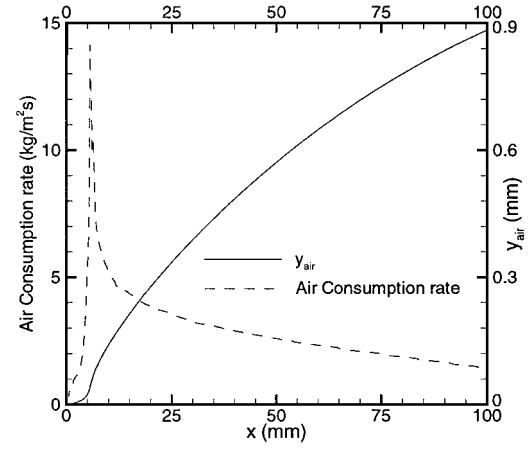

Fig. 10 Case 1 (base case): y_{air} and air consumption rate.

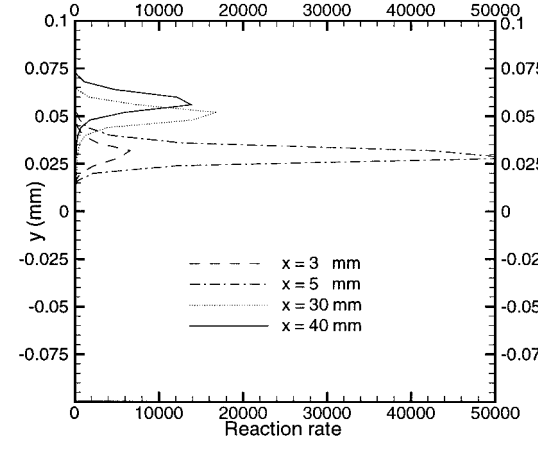

Fig. 11 Reaction rate vs y at different x positions for case 1 (base case).

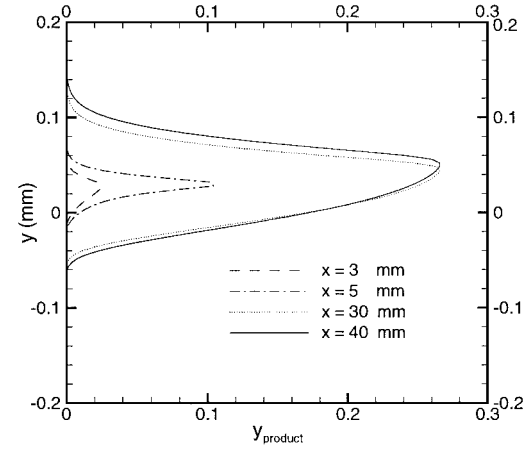

Fig. 12 Product mass fraction vs y at different x positions for case 1 (base case).

value generally is less than 0.1%, except near $x = 1.75$ mm at a few points, the maximum value goes up to 14%. It means that the boundary-layer approximation is adequate everywhere, including the upstream ignition region.

Effect of Pressure Gradient

Table 1 summarizes results for $dp/dx = 0$ atm/m (case 2) and $dp/dx = -350$ atm/m (case 3), respectively. Other parameters remain the same as in the base case. With the increase of the absolute value of the pressure gradient, the ignition distance increases. This results from the increase in flow acceleration with the increased

pressure gradient. That may influence ignition distance in two aspects: 1) Diffusion is less due to lower temperature, which in turn is due to higher velocity. 2) The time needed to reach a certain point downstream is shorter due to higher velocity.

Also, the highest temperature is lower in the case of higher pressure gradient, and the flame thickness is decreasing with the increase of the absolute value of the pressure gradient. The temperature decreases due to higher velocity, and at the same time, less time for diffusion can also decrease flame thickness.

Ignition Distance

There are many parameters that can influence the ignition process and flame structure; we introduce two dimensionless parameters $(-\mathrm{d}p/\mathrm{d}x)(1/p_0)x_{\mathrm{ch}}$ and x_{ig}/x_0, where x_0 is ignition length at $\mathrm{d}p/\mathrm{d}x = 0$, to show some of the influences.

Chemical distance x_{ch} is calculated by using Eq. (23) and the parameters at the initial upper freestream. Here, we define ignition distance as the distance from the flat plate to the first x grid point, where the local peak temperature at that point differs from the local peak temperature at the next x grid point by greater than 3 K. It means the temperature begins to grow very fast at that location.

The dimensionless ignition parameter is varied by keeping p_0 and T_0 constant and changing $\mathrm{d}p/\mathrm{d}x$. Figure 13 shows the dimensionless ignition distance vs the dimensionless ignition parameter for $p_0 = 30$, 60, and 200 atm/m and $T_0 = 2000$ K, which correspond to cases 1, 4, 5, and 6, respectively. Other parameters are the same as in the base case. Figure 13 shows that the dimensionless ignition distance x_{ig}/x_0, where x_0 is ignition at $\mathrm{d}p/\mathrm{d}x = 0$, increases monotonically with the increase of the dimensionless ignition parameter $(\mathrm{d}p/\mathrm{d}x)(1/p_0)x_{\mathrm{ch}}$ in all cases.

Effect of Initial Pressure

Initial pressure also has a significant influence on ignition process. Consider the values for initial pressure $p_0 = 60$ atm (case 4) and $p_0 = 200$ atm (case 5), respectively. The calculations indicate that the higher the initial pressure is, the thinner the mixing layer is. That happens because, when the initial pressure is high, the density is high, the kinematic viscosity $\nu = \mu/\rho$ is smaller, and flow diffuses slower. The dependence on intial pressure in Fig. 13 is not monotonic. An increase to $p_0 = 60$ atm reduces generally the ignition distance, whereas an increase to 200 atm lengthens that distance. Realize that the chemical rate for mass conversion is independent of the pressure for the chosen fuel. As pressure increases, the mass diffusivity decreases thereby inhibiting the onset of ignition by this effect alone. This appears to explain the increase in the ignition length as we vary an initial pressure of 30–60 atm. However, another opposite effect is that, for a given pressure gradient and initial velocity, increases in the initial pressure and density reduce the acceleration and velocity gradient. Therefore, the flow expansion and reduction of temperature are reduced. By this mechanism, ignition length can decrease. This effect apparently dominates as the pressure is increased to 200 atm.

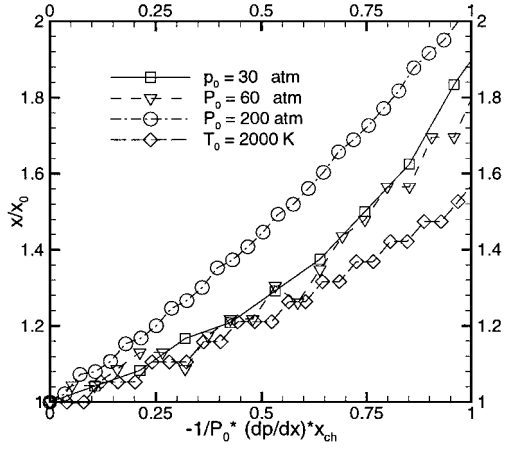

Fig. 13 Dimensionless ignition distance vs dimensionless ignition parameter.

Effect of Initial Temperature

Consider the flowfield for initial air temperature $T_{\mathrm{air}} = 2000$ K (case 6) and for initial fuel temperature $T_F = 700$ K (case 7). The most important influence is the ignition distance; the higher the initial temperature is, the shorter the ignition distance is. The highest temperature and the thickness of the high-temperature zone depends on the initial temperature, too. When the initial temperature is higher, the value of the highest temperature is greater, and the high temperature zone is thicker.[26]

Effects of Other Parameters

Next we can determine the flowfields for initial air velocity $u_{\mathrm{air}} = 100$ m/s (case 8) and initial fuel velocity $u_F = 100$ m/s (case 9). When the initial air velocity u_{air} is increased, the ignition distance increases. An increase in the fuel velocity, however, results in faster diffusion of fuel vapor across the layer and reduces ignition length.

Consider a decrease of the viscosity coefficient μ by a factor of 5 (case 10). The ignition distance is a little shorter, and the shear layer is much thinner. When we decrease the viscosity coefficient, we decrease kinematic viscosity $\nu = \mu/\rho$, which is important to the thickness of the mixing layer.

When we decrease the chemical reaction rate by a factor of 10 (case 11), the ignition distance increases, and the highest temperature is lower. In the ignition region, both chemical rate and diffusion are controlling phenomena. In the downstream region with a fully established flame, the diffusion is rate controlling.

VI. Coupled Study

In this section, we will study the influence of different parameters in a coupled way. When the initial pressure or initial temperature varies, the initial air fraction in the airflow is also changed correspondingly.

Assume that the hot air mixed with burned gases flowing above the flat plate was produced by a chemical reaction of air and CH_4, which is compressed to the initial pressure 30 atm from the reference temperature 298 K and the reference pressure 1.0 atm. After the reaction, the temperature of the products is elevated to the initial temperature T_0. The combustion process of this reaction is described by a one-step overall chemical reaction as

$$\mathrm{CH_4} + 2(1+x)\mathrm{O_2} + 7.52(1+x)\mathrm{N_2} \longrightarrow \mathrm{CO_2} + 2\mathrm{H_2O} + 7.52(1+x)\mathrm{N_2} + 2x\mathrm{O_2}$$

In the base case, corresponding to an initial temperature $T_0 = 1650$ K and an initial pressure $p_0 = 30$ atm, the initial air fraction is $Y_{\mathrm{air}} = 0.5848$.

Figure 14 shows temperature contours for case 12. The highest temperature is lower compared with Fig. 5, which describes the case

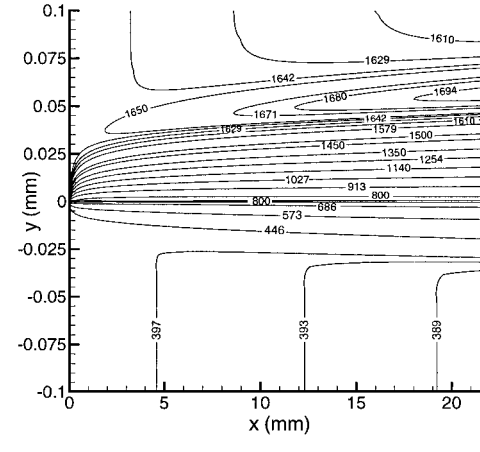

Fig. 14 Temperature contours for case 14 ($Y_{\mathrm{air}} = 0.5848$).

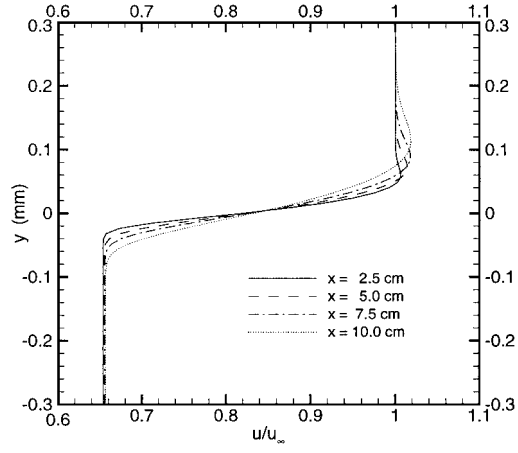

Fig. 15 Dimensionless velocity u/u_∞ vs y at different x positions for case 14 ($Y_{air} = 0.5848$).

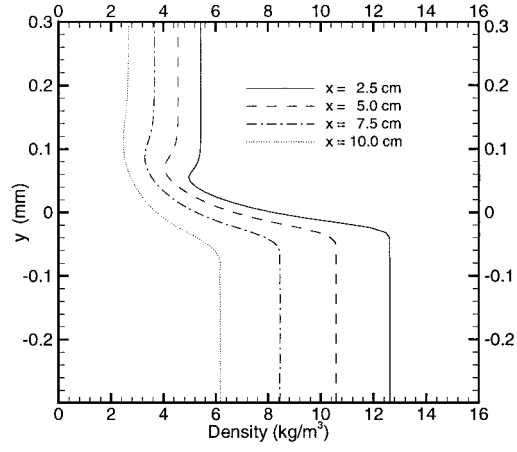

Fig. 16 Density vs y at different x positions for case 14 ($Y_{air} = 0.5848$).

with air fraction $Y_{air} = 1.0$, because the upper freestream air fraction decreases and so does the chemical reaction rate. We can see that the ignition distance is longer; the reason is the same as mentioned earlier. Figure 15 shows the dimensionless velocity u/u_∞ vs y at four different x positions. They are similar to the case in which the air fraction is 1.0. However, the peak value of u/u_∞ is much less than the peak value for case 1 in which the upper freestream air fraction is 1.0. The ignition is much slower and the peak temperature is much lower. Both are due to the slower chemical reaction rate. Figure 16 shows density vs y at four different x positions. As a result of lower peak temperature value compared with case 1, the minimum density value is not as low as in Fig. 6 for case 1.

Figure 17 shows the mass fraction vs y at $x = 10.0$ cm for case 12. The peak value of the product mass fraction also occurs at a positive value of y. Near that point, O_2 and fuel mass fractions decrease fast. In this case, O_2 mass fraction does not decrease across the layer as fast as in case 1, and there is no local minimum value as in case 1 either. This is caused by slower chemical reaction rate due to low air fraction.

Initial pressure also has significant influence on ignition process. Consider two new values for initial pressure, $p_0 = 60$ atm (case 13) and $p_0 = 200$ atm (case 14). Assume that the hot air mixed with burned gases flowing above the flat plate was produced by a chemical reaction of air and CH_4, which is compressed to the specified initial pressure from the reference temperature 298 K and the reference pressure 1.0 atm. After the reaction, the temperature of the products is elevated to an initial air temperature of 1650 K. When corresponding to an initial pressure $p_0 = 60$ atm, the initial air fraction is $Y_{air} = 0.6625$, whereas corresponding to the initial pressure $p_0 = 200$ atm, the initial air fraction is $Y_{air} = 0.8500$.

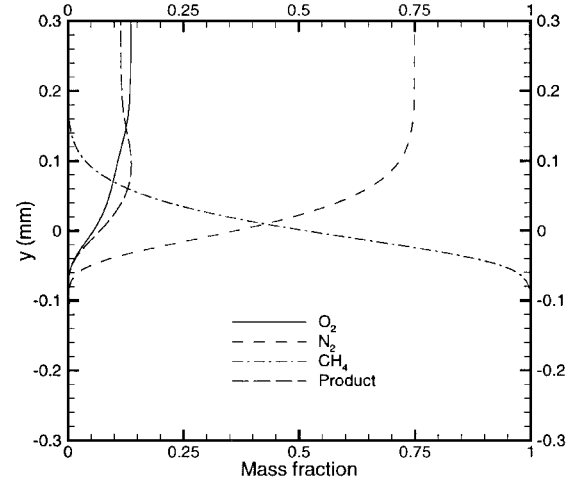

Fig. 17 Mass fraction vs y at $x = 10$ cm for case 14 ($Y_{air} = 0.5848$).

The higher the initial pressure is, the thinner the mixing layer is. When the initial pressure is high, the density is high, the viscosity $\nu = \mu/\rho$ is smaller, and the flow diffuses slower. The same two opposite mechanisms of reduced mass diffusivity and reduced acceleration and expansion that appeared in the uncoupled study do again cause a nonmonotonic behavior for the ignition length. That length increases as the initial pressure is raised to 60 atm. Then it decreases as the pressure increases to 200 atm.

Finally, we consider an initial air temperature $T_{air} = 2000$ K (case 15). In this case, corresponding to the initial temperature $T_0 = 2000$ K and initial pressure $p_0 = 30$ atm, the initial air fraction is $Y_{air} = 0.5848$. The ignition distance is shorter than in case 12. Although the initial air fraction is less in this case, the high air temperature helps the ignition. The ignition distance is still longer than that in case 6, where the initial temperature is also 2000 K but air fraction in the freestream is 1.

VII. Conclusions

Ignition and combustion processes in a transonic accelerating mixing layer have been studied by a finite difference method. The method has been validated against similarity solutions and has been extended to nonsimilar solutions. Although there is some quantitative error in using the chemical rate law given by Eq. (23) for both the ignition and the fully established flame ranges, we expect the trends caused by changes in the flow properties to be properly identified.

The ignition first takes place on the high-temperature-air side of the mixing layer. Fuel vapor must diffuse across the mixing layer to ignite. Any modification that increases the temperature, the fuel vapor concentration, or the residence time in the ignition region will decrease ignition length. Therefore, ignition length decreases as thermal conductivity decreases, as air velocity decreases, as mass diffusivity increases, as fuel velocity increases, or as initial temperature increases. Increased pressure gradient results in more rapid expansion and temperature reduction with an increase in the ignition length.

The effect of initial pressure on the ignition distance is more complex with two opposing effects. Mass diffusivity decreases while pressure increases. Flow acceleration rate also decreases, for a given pressure gradient with an increase in initial pressure and density. The former effect inhibits ignition, whereas the latter enhances it, thereby causing a nonmonotonic dependence of the initial pressure. The upstream region, where ignition occurs, has two processes with comparable rates: oxidation kinetics and mass diffusion. The product layer and reaction zone have comparable thicknesses there. Farther downstream, the flame is fully established, and the diffusion layer thickness is much greater than the reaction zone thickness. Clearly, diffusion is rate controlling there. The boundary-layer approximation is found to be adequate everywhere, including the upstream ignition region. That is, diffusion rates in the flow direction are found

to be generally negligible compared to transverse diffusion rates. With a different chemical kinetic scheme, the pressure sensitivity of the conversion rate could be modified.

The results for the coupled and the uncoupled studies are in quantitative agreement. The effect of initial pressure for methane study should not be generalized because with the methane one-step kinetics, the reaction is of order unity. The laminar mixing layer thickness in these studies are typically submillimeter in size. More practical configurations are expected to be turbulent with much thicker layers as a consequence.

In the presence of accelerating pressure gradients, the maximum velocity and temperature occur near the middle of the shear layer. It is possible that, in an accelerating flow, the flame region is subsonic while the freestreams are supersonic.

The acceleration results in decreasing flame temperature with downstream distance. The analysis leads to the conclusion that substantial potential exists for the reduction of NO_x formation and decreases in heat transfer losses due to the peak temperature reduction. Extinction also becomes possible in some cases. More complete results can be found in Ref 26. Because we use the actual finite chemical kinetics, it is possible to explore pollutant formations or extinction in the future.

Acknowledgments

The authors thank the National Science Foundation for its support for this research under Grant CTS-9714930. The Grant Manager is Farley Fisher.

References

[1]Sirignano, W. A., and Liu, F., "Performance Increases for Gas-Turbines Through Combustion Inside the Turbine," *Journal of Propulsion and Power*, Vol. 15, No. 1, 1999, pp. 111–118.

[2]Liu, F., and Sirignano, W. A., "Turbojet and Turbofan Engine Performance Increases Through Turbine Burners," *Journal of Propulsion and Power*, Vol. 17, No. 3, 2001, pp. 695–705; also AIAA Paper 2000-741, 2000.

[3]Marble, F. E., and Adamson, T. C., Jr., "Ignition and Combustion in a Laminar Mixing Zone," *Jet Propulsion*, Vol. 24, 1954, p. 85.

[4]Emmons, H. W., "Thin Film Combustion of Liquid Fuel," *Zeitschrift für Angewante Mathematik und Mechanik*, Vol. 36, 1956, p. 60.

[5]Chung, P. M., "Chemically Reacting Nonequillibrium Boundary Layers," *Advances in Heat Transfer*, edited by J. P. Hartnett and T. F. Irvine Jr., Academic Press, New York, 1965, pp. 109–270.

[6]Sharma, O. P., and Sirignano, W. A., "On the Ignition of a Pre-Mixed Fuel by a Hot Projectile," *Combustion Science and Technology*, Vol. 1, No. 6, 1970, pp. 481–494.

[7]Patankar, S. V., and Spalding, D. B., *Heat and Mass Transfer in Boundary Layers*, Intertext, London, 1970, pp. 49–57.

[8]Razdan, M. K., and Kuo, K. K., "Erosive Burning Study of Composite Solid Propellants by Turbulent Boundary-Layer Approach," *AIAA Journal*, Vol. 18, No. 11, 1979, pp. 1225–1233.

[9]Givi, P., Ramos, J. I., and Sirignano, W. A., "Probability Density Function Calculations in Turbulent Chemically Reacting Round Jets, Mixing Layers and One-Dimensional Reactors," *Journal of Non-Equilibrium Thermodynamics*, Vol. 10, 1985, pp. 75–104.

[10]Buckmaster, J., Jackson, T. L., and Kumar, A., *Combustion in High-Speed Flows*, Kluwer Academic, Dordrecht, The Netherlands, 1994, pp. 131–252.

[11]Grosch, C. E., and Jackson, T. L., "Ignition and Structure of a Laminar Diffusion Flame in a Compressible Mixing Layer with Finite Rate Chemistry," *Physics of Fluids A*, Vol. 3, No. 12, 1991, pp. 3087–3097.

[12]Jackson, T. L., and Hussaini, M. Y., "An Asymptotic Analysis of Supersonic Reacting Mixing Layers," *Combustion Science and Technology*, Vol. 57, No. 4–6, 1988, pp. 129–140.

[13]Im, H. G., Chao, B. H., Bechtold, J. K., and Law, C. K., "Analysis of Thermal Ignition in the Supersonic Mixing Layer," *AIAA Journal*, Vol. 32, No. 2, 1994, pp. 341–349.

[14]Im, H. G., Helenbrook, B. T., Lee, S. R., and Law, C. K., "Ignition in the Supersonic Hydrogen/Air Mixing Layer with Reduced Reaction Mechanisms," *Journal of Fluid Mechanics*, Vol. 322, 1996, pp. 275–296.

[15]Chakraborty, D., Upadhyaya, H. V. N., Paul, P., and Mukunda, H., "A Thermochemical Exploration of a Two-Dimensional Reacting Supersonic Mixing Layer," *Physics of Fluids*, Vol. 9, No. 11, 1997, pp. 3512–3522.

[16]Li, T. Y., and Nagamatsu, H. T., "Similar Solutions of Compressible Boundary Layer Equations," *Journal of the Aeronautical Sciences*, Vol. 20, 1953, pp. 653–655.

[17]Cohen, C. B., "Similar Solutions of Compressible Laminar Boundary Layer Equations," *Journal of the Aeronautical Sciences*, Vol. 21, 1954, pp. 281, 282.

[18]Cohen, C. B., and Reshotko, E., "The Compressible Laminar Boundary Layer with Heat Transfer and Arbitrary Pressure Gradient," NACA Rept. 1294, 1956.

[19]Illingworth, C. R., "Steady Flow in the Laminar Boundary Layer of a Gas," *Proceedings of the Royal Society of London, Series A: Mathematical and Physical Sciences*, Vol. 199, 1949, pp. 533–558.

[20]Stewartson, K., "Correlated Compressible and Incompressible Boundary Layers," *Proceedings of the Royal Society of London, Series A: Mathematical and Physical Sciences*, Vol. 200, 1949, pp. 84–100.

[21]Schlichting, H., *Boundary Layer Theory*, McGraw–Hill, New York, 1979, p. 340.

[22]Sirignano, W. A., and Kim, I., "Diffusion Flame in a Two-Dimensional, Accelerating Mixing Layer," *Physics of Fluids*, Vol. 9, No. 9, 1997, pp. 2617–2630.

[23]White, F. M., *Viscous Fluid Flow*, 2nd ed., McGraw–Hill, New York, 1991, p. 28.

[24]Fletcher, C. A. J., *Computational Techniques for Fluid Dynamics*, Vol. 1, 2nd ed., Springer-Verlag, New York, 1990, pp. 305, 306.

[25]Westbrook, C. K., and Dryer, F. L., "Chemical Kinetic Modeling of Hydrocarbon Combustion," *Progress in Energy and Combustion Science*, Vol. 10, No. 1, 1984, pp. 1–57.

[26]Fang, X., "Ignition and Flame Studies for an Accelerating Transonic Mixing Layer," M.S. Thesis, Dept. of Mechanical and Aerospace Engineering, Univ. of California, Irvine, CA, Dec. 1999.